



AFRL-RQ-WP-TP-2014-0131

STUDY OF A MULTI-PHASE HYBRID HEAT EXCHANGER-REACTOR (HEX REACTOR): PART II – NUMERICAL PREDICTION OF THERMAL PERFORMANCE (POSTPRINT)

Nicholas Niedbalski and Debjyoti Banerjee

Texas A&M University

Douglas Johnson

University of Dayton Research Institute

Soumya S. Patnaik

Mechanical and Thermal Systems Branch

Power and Control Division

NOVEMBER 2013

Approved for public release; distribution unlimited.

See additional restrictions described on inside pages

STINFO COPY

**AIR FORCE RESEARCH LABORATORY
AEROSPACE SYSTEMS DIRECTORATE
WRIGHT-PATTERSON AIR FORCE BASE, OH 45433-7542
AIR FORCE MATERIEL COMMAND
UNITED STATES AIR FORCE**

NOTICE AND SIGNATURE PAGE

Using Government drawings, specifications, or other data included in this document for any purpose other than Government procurement does not in any way obligate the U.S. Government. The fact that the Government formulated or supplied the drawings, specifications, or other data does not license the holder or any other person or corporation; or convey any rights or permission to manufacture, use, or sell any patented invention that may relate to them.

This report was cleared for public release by the USAF 88th Air Base Wing (88 ABW) Public Affairs Office (PAO) and is available to the general public, including foreign nationals.

Copies may be obtained from the Defense Technical Information Center (DTIC) (<http://www.dtic.mil>).

AFRL-RQ-WP-TP-2014-0131 HAS BEEN REVIEWED AND IS APPROVED FOR PUBLICATION IN ACCORDANCE WITH ASSIGNED DISTRIBUTION STATEMENT.

**//Signature//*

TRAVIS E MICHALAK
Program Manager
Mechanical and Thermal Systems Branch
Power and Control Division

//Signature//

THOMAS L. REITZ, Technical Advisor
Mechanical and Thermal Systems Branch
Power and Control Division
Aerospace Systems Directorate

//Signature//

JOHN G. NAIRUS, Chief Engineer
Power and Control Division
Aerospace Systems Directorate

This report is published in the interest of scientific and technical information exchange, and its publication does not constitute the Government's approval or disapproval of its ideas or findings.

Disseminated copies will show “//Signature//*” stamped or typed above the signature blocks.

REPORT DOCUMENTATION PAGE				<i>Form Approved</i> OMB No. 0704-0188	
<p>The public reporting burden for this collection of information is estimated to average 1 hour per response, including the time for reviewing instructions, searching existing data sources, gathering and maintaining the data needed, and completing and reviewing the collection of information. Send comments regarding this burden estimate or any other aspect of this collection of information, including suggestions for reducing this burden, to Department of Defense, Washington Headquarters Services, Directorate for Information Operations and Reports (0704-0188), 1215 Jefferson Davis Highway, Suite 1204, Arlington, VA 22202-4302. Respondents should be aware that notwithstanding any other provision of law, no person shall be subject to any penalty for failing to comply with a collection of information if it does not display a currently valid OMB control number. PLEASE DO NOT RETURN YOUR FORM TO THE ABOVE ADDRESS.</p>					
1. REPORT DATE (DD-MM-YY) November 2013		2. REPORT TYPE Journal Article Postprint		3. DATES COVERED (From - To) 01 October 2011 – 28 May 2013	
4. TITLE AND SUBTITLE STUDY OF A MULTI-PHASE HYBRID HEAT EXCHANGER-REACTOR (HEX REACTOR): PART II – NUMERICAL PREDICTION OF THERMAL PERFORMANCE (POSTPRINT)				5a. CONTRACT NUMBER In-house	
				5b. GRANT NUMBER	
				5c. PROGRAM ELEMENT NUMBER 62203F	
6. AUTHOR(S) Nicholas Niedbalski and Debjyoti Banerjee (Texas A&M University) Douglas Johnson (University of Dayton Research Institute) Soumya S. Patnaik (AFRL/RQQM)				5d. PROJECT NUMBER 3145	
				5e. TASK NUMBER N/A	
				5f. WORK UNIT NUMBER Q0LA	
7. PERFORMING ORGANIZATION NAME(S) AND ADDRESS(ES) Texas A&M University Department of Mechanical Engineering 3123 TAMU College Station, TX 77843 ----- University of Dayton Research Institute 300 College Park Dayton, OH 45469			8. PERFORMING ORGANIZATION REPORT NUMBER AFRL-RQ-WP-TP-2014-0131		
9. SPONSORING/MONITORING AGENCY NAME(S) AND ADDRESS(ES) Air Force Research Laboratory Aerospace Systems Directorate Wright-Patterson Air Force Base, OH 45433-7542 Air Force Materiel Command United States Air Force				10. SPONSORING/MONITORING AGENCY ACRONYM(S) AFRL/RQQM	
				11. SPONSORING/MONITORING AGENCY REPORT NUMBER(S) AFRL-RQ-WP-TP-2014-0131	
12. DISTRIBUTION/AVAILABILITY STATEMENT Approved for public release; distribution unlimited.					
13. SUPPLEMENTARY NOTES PA Case Number: 88ABW-2013-2498; Clearance Date: 28 May 2013. Report published in <i>International Journal of Heat and Mass Transfer</i> 70 (2014). The U.S. Government is joint author of the work and has the right to use, modify, reproduce, release, perform, display, or disclose the work.					
14. ABSTRACT Numerical models were developed to assess the thermal performance of a HEX reactor with solid-to-gas reacting flow. Based on the experimental results obtained in part I of this study, numerical models were developed to predict the thermal performance of a plate heat exchanger-based HEX reactor involving multi-phase flow with chemical reactions. A reduced-order numerical model of a chevron plate heat exchanger was developed with thermal and momentum transfer analogies. Empirical correlations for momentum transfer and void fraction (validated in part I of this study) were implemented in the numerical model. The numerical model, coded in Maple 13™, was used to size a compact reactor with a thermal load rating of 2 kW for the desired operating temperature; the modeling framework developed can also be used to study different candidate gas-generating reacting species, working fluids, and PHE configurations.					
15. SUBJECT TERMS ammonium carbamate, HEX Reactor, thermal management, plate heat exchanger, reacting flow, multi-phase flow					
16. SECURITY CLASSIFICATION OF:			17. LIMITATION OF ABSTRACT: SAR	18. NUMBER OF PAGES 16	19a. NAME OF RESPONSIBLE PERSON (Monitor) Travis E. Michalak 19b. TELEPHONE NUMBER (Include Area Code) N/A
a. REPORT Unclassified	b. ABSTRACT Unclassified	c. THIS PAGE Unclassified			



Study of a multi-phase hybrid heat exchanger-reactor (HEX reactor): Part II – Numerical prediction of thermal performance



Nicholas Niedbalski^{a,b,*}, Douglas Johnson^c, Soumya S. Patnaik^a, Debjyoti Banerjee^b

^aAir Force Research Laboratory, Aerospace Systems Directorate, Power and Controls Division, Mechanical and Thermal Systems Branch, 1950 5th St., Wright-Patterson AFB, OH 45433, United States

^bTexas A&M University, Department of Mechanical Engineering, 3123 TAMU, College Station, TX 77843, United States

^cUniversity of Dayton Research Institute, 300 College Park, Dayton, OH 45469, United States

ARTICLE INFO

Article history:

Available online 16 November 2013

Keywords:

Ammonium carbamate
HEX reactor
Thermal management
Plate heat exchanger
Reacting flow
Multi-phase flow

ABSTRACT

Numerical models were developed to assess the thermal performance of a HEX reactor with solid-to-gas reacting flow. Based on the experimental results obtained in part I of this study, numerical models were developed to predict the thermal performance of a plate heat exchanger-based HEX reactor involving multi-phase flow with chemical reactions. A reduced-order numerical model of a chevron plate heat exchanger was developed with thermal and momentum transfer analogies. Empirical correlations for momentum transfer and void fraction (validated in part I of this study) were implemented in the numerical model. The numerical model, coded in Maple 13™, was used to size a compact reactor with a thermal load rating of 2 kW for the desired operating temperature; the modeling framework developed can also be used to study different candidate gas-generating reacting species, working fluids, and PHE configurations.

© 2013 Elsevier Ltd. All rights reserved.

1. Introduction

Chevron PHEs are known to provide high heat transfer coefficients with a high surface area-to-volume ratio [1], enabling high thermal power ratings without incurring significant footprint expenses. The corrugated plate geometry also produces swirling secondary flows and early transition to turbulence at low Re, yielding near-ideal mixing behavior in addition to exceptional thermal performance: for instance, Santacesaria et al. [2] reported higher yields of biodiesel at relatively low Re, which they credited to strong localized micromixing and turbulence. Edge et al. [3] used a model single-phase exothermic reaction to characterize both heat transfer and reactant micromixing performance for a PHE-based HEX reactor. Their results showed reduced byproduct formation indicative of high micromixing.

The results reported in the literature suggest tremendous potential for the HEX reactor scheme introduced in a previous study [4], and discussed in part I of this study. Nevertheless, it is clear that there is a lack of both experimental and theoretical understanding of solid-to-gas reacting flows in a chevron PHE. Consideration of such a unique HEX reactor will require extensive

exploration from an analysis and design standpoint. It is therefore important to develop reliable and accurate models to predict both the thermal performance and conversion efficiency of a given HEX reactor design, in effect providing an initial feasibility test for the HEX reactor's role as a thermal management scheme. There appears to be only a limited number of models developed for chevron PHE-based HEX reactors (such as that developed by Edge et al. [3]), none of which consider multi-phase flows. On the other hand, models developed for chevron PHEs that consider multi-phase flows focus on refrigerant evaporation and/or condensation (e.g., [5,6]), but without chemical reaction. To our knowledge, there are no models proposed in the open literature that are applicable to solid-to-gas reacting flow in a chevron PHE. Hence, the focus of this paper is to develop a computer model for the coupled heat, momentum, mass transfer, and chemical kinetics of an endothermic solid-gas reaction in a chevron PHE. The model predictions for thermal-hydraulic performance were used to demonstrate the utility of the solid-gas endothermic HEX reactor for thermal management. Calculations were performed using the void fraction and two-phase multiplier correlations that were experimentally validated in part I. Thermal performance estimates were obtained using a modified heat/momentum transfer analogy from the literature that has been developed for PHEs.

The volumetric energy densities of thermochemical reactions generally exceed that of thermophysical reactions. It has been previously demonstrated [4] that the endothermic solid-to-gas decomposition of ammonium carbamate (AC) holds significant

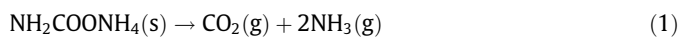
* Corresponding author at: Air Force Research Laboratory, Aerospace Systems Directorate, Power and Controls Division, Mechanical and Thermal Systems Branch, A236, Building 18, 1950 5th St., Wright-Patterson AFB, OH 45433, United States. Tel.: +1 (425) 358 1295.

E-mail address: nickgonzaga@me.com (N. Niedbalski).

Nomenclature

A	surface area	q''	wall heat flux
C	mass concentration	t_{plate}	plate thickness
D	diameter	u	velocity
Da	Damköhler number	\dot{w}	power rating
G	constant in Eq. (3)	x	mass quality
L	length	z	dimensionless axial coordinate
\dot{M}'''	dimensionless reaction rate	z^*	axial coordinate
Nu	Nusselt number		
P	pressure	Greeks	
P_p	partial pressure	Λ	corrugation pitch
Pr	Prandtl number	Θ	dimensionless temperature in Figs. 9 and 10
Q_{latent}	heat rejected to ammonium carbamate	Φ_{AE}	area enlargement factor
Q_{load}	total heat rejected	Φ_{TP}^2	two-phase multiplier
R	heat capacity ratio	α	void fraction
Re	Reynolds number	β	chevron angle
T	temperature	θ	dimensionless temperature
T^*	normalized load temperature	ε	Q_{latent}/Q_{load}
T_{ld}^*	load temperature at full conversion	κ	rate constant
U	superficial velocity	η	dimensionless concentration
V	volume	ρ	density
W	plate width (between gasket)		
X	Lockhart–Martinelli parameter	Subscripts	
		A	acceleration
Lowercases		F	friction
a	rate constant in Eq. (2)	G	gravity
d	½ corrugation depth	SP	single-phase
c_p	specific heat capacity	TP	two-phase
e	constant in Eq. (3)	c	corrugated section
f	Darcy friction factor	e	equivalent
g	gravitational acceleration	eq	at equilibrium
h	convection coefficient	g	gas phase
$1/h_{eff}$	overall thermal resistance	h	hydraulic
i	cell index	in	value at inlet
k	thermal conductivity	ld	liquid phase, load side
k_{plate}	thermal conductivity of plate	ls	liquid phase, slurry side
\dot{m}'''	volumetric reaction rate	p	AC particle
\dot{m}''_{total}	total mass flux	pp	port-to-port
n	channel index		

potential as a high energy density thermochemical heat sink for thermal management. AC is a salt that is readily available in powder form as a cheap byproduct of urea synthesis [7]. AC undergoes a reversible solid–gas decomposition reaction, shown below:



Despite the low operating temperature ($\sim 70^\circ\text{C}$) and high energy density (2000 kJ/kg), the impediment to AC in a practical thermal management system is its low thermal conductivity ($\sim 0.4\text{ W/m K}$) [7]. This presents a significant barrier to conducting thermal energy in bulk AC salt. Schmidt [7] proposed forming reacting slurry by immersing small AC salt particles in a non-reactive heat transfer fluid (HTF) to overcome this impediment. Previous research [8,9] demonstrated successful use of PHEs with slurries containing thermophysical phase-change materials (PCM). However, due to the high enthalpy of decomposition, AC can enable higher overall energy density to be achieved than with the thermophysical PCM slurries considered in the aforementioned studies.

2. Mathematical analysis

Gasketed chevron PHEs are a stack of channels formed by thin corrugated heat transfer plates which are separated by gaskets. The corrugations are aligned in a repeating series of chevrons to

form an oblique, wavy surface. A discussion of the background of PHEs is provided by Johnson et al. [4] and in part I of this study. The geometric characteristics of the PHE used in this study are depicted in Fig. 1.

A schematic of the HEX reactor architecture considered in this study is shown in Fig. 2. A hot stream fluid delivers heat to the cold stream fluid carrying suspended AC; the PHE has a single-pass, parallel, vertical upflow arrangement. The model developed in this study considers the PHE to comprise of a stack of equivalent flat plates, forming a collection of N channels as illustrated in Fig. 2. Each channel is represented by a ‘submodel’ whose interaction with other submodels in the system is defined by appropriate boundary conditions, as illustrated in Fig. 3. In the case considered here, channel submodels are permitted to interact by exchanging thermal energy. The heat transfer coefficient, friction factor, two-phase multiplier, and void fraction are estimated by employing empirical correlations obtained from the literature.

This approach is based on the idea of hierarchical modeling, which has been previously employed for the analysis of PHE performance in industrial applications [10]. The treatment of individual channels as separate submodels (Fig. 3) also allows for non-idealities seen in real heat exchangers, such as maldistribution of flow patterns, to be incorporated into the overall reactor model (Fig. 2).

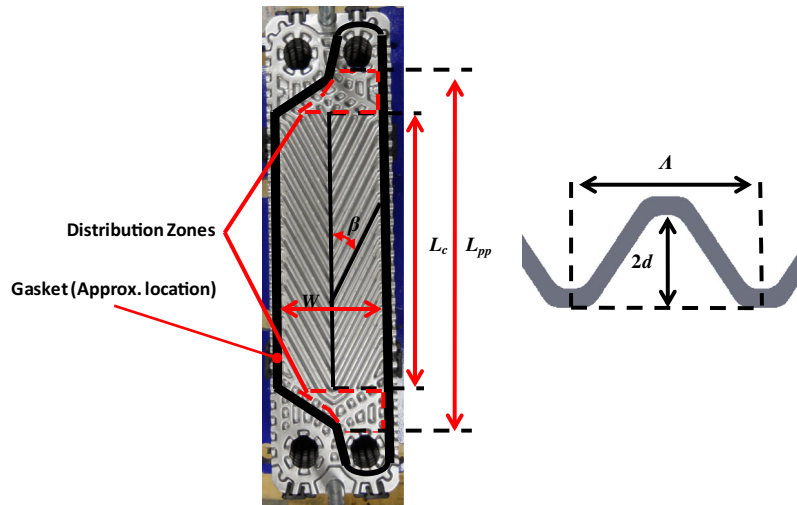


Fig. 1. (Left) Image of a representative chevron PHE heat transfer plate (Alpha Laval MF3) used in this study. (Right) Wavy corrugation profile observed in side view.

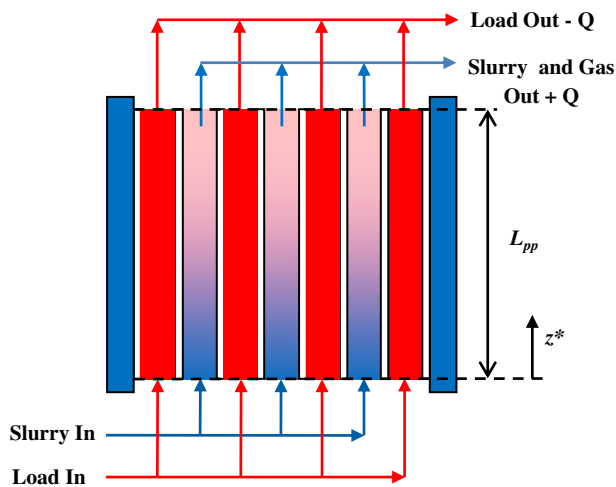


Fig. 2. Schematic of reactor flow arrangement.

- Due to the small particle size, the contribution of the suspended solids on the momentum equation is negligible [12] (i.e., the small concentration of the tiny suspended particles does not cause appreciable change in the effective viscosity and rheological properties of the bulk liquid phase).
- Reduced order models involving one-dimensional equivalent flows are used; i.e., cross-sectional variation in the temperature, velocity, and void fraction profiles are replaced by area averaged quantities.
 - o Primary flow variables are permitted to differ between the liquid and gas phases (separated flow model).
 - o Heat transfer to the gas phase is negligible when compared to heat transferred to the liquid phase and the suspended AC. This is a reasonable engineering approximation due to the short residence times and the low thermal conductivity values of the gas phase compared to that of the liquid phase.
- The reaction occurs at the local bulk temperature due to homogeneous mixing produced by bubble agitation and secondary flows characteristic of PHEs.
- Negligible conduction heat transfer in the axial direction.
- Fluids are Newtonian and incompressible.

2.1. Transport equations

The separated flow model [11] is used for developing the transport equations of energy, mass, and momentum for the liquid and gas phases in the multi-phase flow configuration, wherein the gas phase and liquid phase (heat transfer fluid and suspended solid) are considered segregated. The mutual interactions between gas and liquid phase are estimated using appropriate experimental correlations (validated from the experiments conducted in part I of this study).

Some of the assumptions used in the HEX reactor model are listed as follows:

- Steady-state operation (using time averaged values).
- The gas mixtures (reaction products) are insoluble in the liquid phase.
- No evaporation occurs in the liquid phase on the slurry side.
- The flow is approximated as a pseudo two-phase flow (homogeneous flow model for the AC in the liquid) where the liquid “solution” of AC (rather than a collection of discrete particles) is considered to undergo uniform volumetric heat generation (or heat sink) due to homogeneously distributed volumetric chemical reactions and mass concentration at a given axial location.

In accordance with the aforesaid assumptions, an integral mass, species, energy, and momentum balance on a 1-dimensional control volume yields the following governing equations:

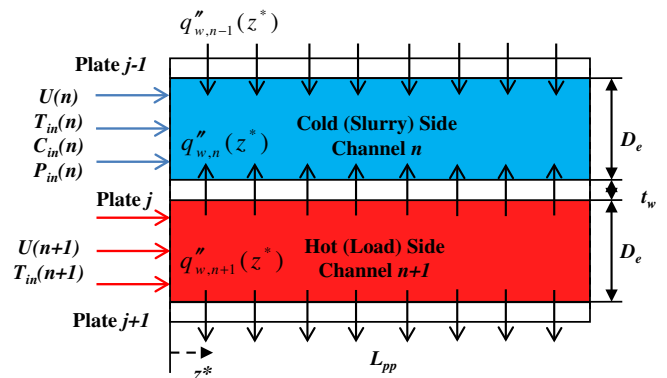


Fig. 3. Interaction between channel submodels.

2.1.1. Continuity

$$u_{ls,n} = \frac{U_{ls,n}}{1 - \alpha_n} \quad (2)$$

$$u_{g,n} = \frac{U_{ls,n}(C_{in,n} - C_n)}{\rho_{g,n}\alpha_n} \quad (3)$$

where u is the velocity (m/s), U is the superficial velocity (m/s), ρ is the density (kg/m³), and C is the mass concentration of solid AC (kg/m³) per unit volume of liquid slurry.

2.1.2. Species

$$U_{ls} \frac{dC_n}{dz^*} = -\dot{m}_n'''(1 - \alpha_n) \quad (4)$$

where \dot{m}_n''' is the volumetric reaction rate (kg/m³ s) per unit volume of liquid slurry.

2.1.3. Energy

$$U_{ls,n} \frac{dT_n}{dz^*} = -\frac{\Delta H}{\rho_{ls}c_{p,ls}} \dot{m}_n'''(1 - \alpha_n) + \frac{q_n'' + q_{n-1}''}{D_e \rho_{ls} c_{p,ls}} \quad (5)$$

$$U_{ld,n} \frac{dT_n}{dz^*} = \frac{q_n'' + q_{n-1}''}{D_e \rho_{ld} c_{p,ld}} \quad (6)$$

where T is the temperature (K), q'' is the wall heat flux (W/m²), c_p is the specific heat capacity (J/kg K), and D_e is the equivalent diameter (m, twice the corrugation amplitude). The momentum equation splits the total pressure gradient into frictional, hydrostatic, and acceleration components [11]:

2.1.4. Momentum

$$\frac{dP_n}{dz^*} = \frac{dP_{F,n}}{dz^*} + \frac{dP_{G,n}}{dz^*} + \frac{dP_{A,n}}{dz^*} \quad (7)$$

where,

$$\frac{dP_{A,n}}{dz^*} = u_{ls,n} \rho_{ls} (1 - \alpha_n) \frac{du_{ls,n}}{dz^*} + u_{g,n} \rho_{g,n} \alpha_n \frac{du_{g,n}}{dz^*} \quad (8)$$

$$\frac{dP_{G,n}}{dz^*} = g[(1 - \alpha_n) \rho_{ls} + \alpha_n \rho_{g,n}] \quad (9)$$

$$\frac{dP_{F,n}}{dz^*} = \frac{(f \rho U^2)_{ls,n}}{2D_h} \Phi_{TP,n}^2 \quad (10)$$

where g is the gravitational acceleration (m/s²), D_h is the hydraulic diameter (m). The subscript n is used to indicate that the respective quantity may vary from channel to channel. Inlet temperatures, pressures, concentrations, and flow rates to each channel are presumed known. Heat transfer between channel submodels n and $n - 1$ is assumed to occur by 1-D heat conduction, as is typical in heat exchanger analysis [1]:

$$q_{n-1}'' = \left[\frac{1}{h_n} + \frac{t_{plate}}{k_{plate}} + \frac{1}{h_{n-1}} \right]^{-1} (T_{n-1} - T_n) = h_{eff,n-1} (T_{n-1} - T_n) \quad (11)$$

where h is the local convection coefficient (W/m² K), t_{plate} is the heat transfer plate thickness (m), and k_{plate} is the thermal conductivity of the plate (W/m K). The end plates are treated as insulated boundaries, since they are much thicker than the plates, and PHEs are designed to minimize heat losses to the environment through the end plates and gaskets [1].

2.2. Incorporation of kinetic model

The current state of knowledge about the kinetics of AC decomposition is quite limited; the open literature offers few mathematical models for the reaction rate. As a starting point, we selected Claudel and Boulamri's [13] net rate model for the decomposition or formation of AC, as provided below:

$$\frac{dP_p}{dt} = a A_p |P_p - P_{eq}|^2 \quad (12)$$

where P_p is the partial pressure (kPa) of the NH₃ and CO₂ evolved during the course of decomposition, a is the rate coefficient (kPa/m² s), and A_p is the surface area of solid AC (m²). The equilibrium pressure, P_{eq} , follows an Arrhenius-type dependence on temperature [14]:

$$P_{eq}(T) = G \exp\left(-\frac{e}{T}\right) \quad (13)$$

where G and e are constants equal to 1.9122×10^{10} kPa and 6321.7 K, respectively, as obtained from Koutinas et al. [14]. Fig. 4 shows a plot of Eq. (13) as a function of temperature, with values measured from various sources in the literature. According to Eq. (13), the minimum operating temperature (under standard atmospheric pressure) for the system is ~ 60 °C. Schmidt [7] also measured the decomposition pressure as a function of temperature for AC immersed in propylene glycol or ethylene glycol, and found no significant departure from the curve described by Eq. (13).

The red arrow in Fig. 4 represents the thermodynamic “driving force” behind the reaction, or “equilibrium drop,” as some authors have used for solid-to-gas reversible reactions [18]. The red dotted line represents the equilibrium vapor pressure corresponding to the local temperature of the solid AC, whereas the black dotted line represents the local partial pressure acting on the reactor contents. Schmidt confirmed that the decomposition rate could be accelerated appreciably by maintaining the AC far from its equilibrium condition, maximizing the equilibrium drop. This driving force is accounted for in Claudel and Boulamri's model. Since the form of Eq. (12) is indicative of a physical mechanism [13], we postulate that the same mechanism will exist even when immersed in a heat transfer fluid.

The rate equation discussed above is incorporated into the species conservation equation via the volumetric reaction term, \dot{m}_n''' .

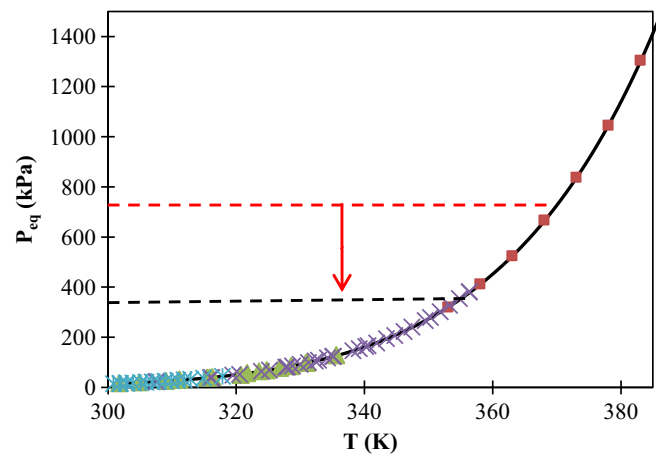


Fig. 4. Dissociation pressure P_{eq} as a function of temperature predicted by Eq. (3) compared with experimental results obtained in the literature. Red squares: Koutinas et al. [14]; green triangles: Bennet et al. [15]; purple X's: Egan and Potts [16]; blue asterisks: Briggs and Migrdichian [17]. (For interpretation of the references to color in this figure legend, the reader is referred to the web version of this article.)

Assuming that the dependence upon surface area and equilibrium drop is the same as that which was proposed by Claudel and Boulamri [13], the decomposition rate of an individual particle is:

$$\frac{d}{dt}(\rho_p V_p) = -\kappa A_p |P_{eq} - P|^2 \quad (14)$$

where V_p is the particle volume (m^3), ρ_p is the particle density (kg/m^3) (assumed to be uniform throughout the particle), and κ is the specific rate coefficient based on surface area, which will assuredly differ from the rate constant calculated in Claudel and Boulamri's study. As an initial approximation, since the variation of NH_3 and CO_2 partial pressures in the HEX reactor has not yet been experimentally investigated, the partial pressure P_p in Eq. (14) is assumed to equal the local static pressure of the liquid, P . P_{eq} is a function of temperature; Schmidt's [7] results for AC in propylene glycol and ethylene glycol match well with the $P_{eq}(T)$ curves obtained in literature for dry AC [14], as described by Eq. (13).

It follows that the mass concentration of solid AC per unit volume of liquid heat transfer fluid is $C = n''' \rho_p V_p$. On a volumetric basis, the rate of solid mass consumption by decomposition may then be written, assuming that the particles are approximately spherical,

$$\dot{m}''' = -\omega \kappa C^{2/3} |P_{eq} - P|^2 \quad (15)$$

where $\omega = (4\pi n''')^{1/3} (3/\rho_p)^{2/3}$. This result can be inserted directly into the cross-sectional average values governing Eqs. (4) and (5), assuming that n''' is constant. In order for such an assumption to hold, the following conditions must be satisfied:

- The particles are evenly distributed, and no agglomeration or break-up into smaller particles occur.
- Particles do not accumulate within the reactor, nor are they completely consumed by the reaction.
- Particles at a given location within the channel are subject to the same local pressure and temperature conditions.

In effect, these assumptions yield a shrinking core-type model wherein only the size of the particles change as the reaction progresses, with the reaction rate tending toward zero as the surface area available for reaction also tends toward zero.

To elucidate the important parameters influencing the solution of the system, a non-dimensional analysis is performed. Introducing the following dimensionless variables and assuming no maldistribution is present:

$$\theta_n = \frac{T_n}{\left(\frac{\Delta H C_{in}}{\rho_{ls} c_{p,ls}}\right)} \quad (16a)$$

$$\eta_n = \frac{C_n}{C_{in}} \quad (16b)$$

$$z = \frac{z^*}{L_{pp}} \quad (16c)$$

$$Da = \frac{\omega \kappa L_{pp}}{C_{in}^{1/3} U_{ls}} |P_{eq}(T_{ld,in}) - P_{atm}|^2 \quad (16d)$$

$$\varphi_n = \frac{L_{pp}}{D_e} \frac{Nu_n}{RePr} \quad (16e)$$

$$R = \frac{(U \rho c_p)_{ls}}{(U \rho c_p)_{ld}} \quad (16f)$$

$$\dot{M}_n''' = \begin{cases} \eta_n^{2/3} \left[\frac{P_{eq}(T_n) - P_n}{P_{eq}(T_{ld,in}) - P_{atm}} \right]^2 & P_{eq} > P \\ 0 & P_{eq} \leq P \end{cases} \quad (16g)$$

The energy equation for the slurry side and load side, respectively, become:

$$\frac{d\theta_n}{dz} = -Da \dot{M}_n''' (1 - \alpha_n) + \varphi_n (\theta_{n+1} - \theta_n) + \varphi_{n-1} (\theta_{n-1} - \theta_n) \quad (17)$$

$$\frac{d\theta_n}{dz} = R_n [\varphi_n (\theta_{n+1} - \theta_n) + \varphi_{n+1} (\theta_{n-1} - \theta_n)] \quad (18)$$

The species conservation equation becomes:

$$\frac{d\eta_n}{dz} = -Da \dot{M}_n''' (1 - \alpha_n) \quad (19)$$

There are three dimensionless groups that arise: a Damköhler number (Da), φ , and heat capacity rate ratio (R). The Damköhler number is a ratio of the timescale of the chemical reaction to the timescale for mass transfer by advection. The group φ , which is a function of axial position, is a dimensionless heat transfer coefficient that relates the magnitude of heat transfer by wall heat flux to heat transfer by advection; the Reynolds number and Prandtl number are evaluated according to the physical properties and superficial velocity of the slurry, and overall thermal resistance is used in place of the convection coefficient in the Nusselt number.

2.3. Correlation selection

There are no correlations available in the literature developed specifically for a reacting multi-phase flow in a chevron PHE. The criteria for selecting empirical correlations to explore the thermo-hydraulic performance should adhere to the following guidelines:

1. Conservative estimates are provided for reactor design.
2. The correlations are applicable to a wide range of geometric parameters for PHEs.

Many heat exchanger correlations are derived from heat and momentum transfer data (i.e., f and Nu) averaged over the entire channel length. However, the quantities to which the said data is correlated will vary with axial position, mostly due to changes in the void fraction and mass quality of the flow. To account for these variations, it is assumed that these correlations may be applied at the prevailing conditions at any axial location z , and integrated over the channel length – in essence, a quasi-equilibrium model.

In this study, a semi-empirical model due to Martin [19] was selected for the single-phase friction factor, since it correlates data for a range of chevron angles fairly well. Martin's model is based on observations gathered from earlier flow visualization studies of the flow patterns inside PHEs [20,21], which showed that two types of flows exist simultaneously: crossing substreams that follow the corrugations, and sinusoidal wavy flow between the upper and lower plate corrugations as the fluid travels down the main flow direction. Martin's model is expressed as [19]:

$$\frac{1}{\sqrt{f}} = \frac{\cos \beta}{\sqrt{0.18 \tan \beta + 0.36 \sin \beta + f_0 \cos \beta}} + \frac{1 - \cos \beta}{\sqrt{3.8 f_1}} \quad (20)$$

where,

$$f_0 = \begin{cases} \frac{64}{Re_h} & Re_h < 2000 \\ (1.8 \ln(Re_h) - 1.5)^{-2} & Re_h \geq 2000 \end{cases} \quad (21)$$

$$f_1 = \begin{cases} \frac{597}{Re_h} + 3.85 & Re_h < 2000 \\ \frac{39}{Re_h^{0.289}} & Re_h \geq 2000 \end{cases} \quad (22)$$

where Re_h is the Reynolds number based on the hydraulic diameter, defined as $D_h = 4b/\Phi_{AE}$, with Φ_{AE} being the area enlargement factor

given by the ratio of the actual surface area to the projected surface area of the corrugated chevron plate.

For two-phase flow, no reports exist on models or correlations specific to the reacting multi-phase flow configurations encountered in this study. The most reasonable example in the literature akin to this situation is that of air–water vertical upward flow, which a limited number of investigators have considered [22–27]. In the reacting slurry, the liquid phase and the gas byproducts do not undergo additional phase changes, and changes in the flow quality only occur through chemical reaction rather than evaporation or condensation. One may imagine an equivalent air–water flow in which gas is continuously introduced along the length of the channel; the implicit assumption in this analogy is that the hydrodynamics of air–water flow is similar to that of the gas evolving reacting flow considered in this study.

Tribbe and Müller-Steinhagen [23,24] studied air–water two-phase vertical upflow in different commercial chevron PHEs having different corrugation depths and chevron angles. These authors found that their frictional pressure drop data, using the appropriate single-phase friction factor, could be well correlated by the relation [24]:

$$\Phi_{TP} = 1.423 - 0.0724 \ln X + 1.031/X \quad (23)$$

where X is the Lockhart–Martinelli parameter, defined as:

$$X = \sqrt{\left(\frac{dP}{dz}\right)_{F,l} / \left(\frac{dP}{dz}\right)_{F,g}} \quad (24)$$

Tribbe and Müller-Steinhagen [24] claim their correlation to be valid within $0.06 < X < 10$. From the experiments conducted in part I of this study, the frictional pressure drop could be adequately described by this correlation when a correction factor of 3.0 was applied. Since the reaction rates of the sodium bicarbonate/acetic acid system are much greater than the decomposition of AC (since the former is mixing-limited), and in the interest of obtaining conservative estimates, the model presented here does not apply this correction factor to Eq. (23). Likewise, following the recommendation of Kreissig and Müller-Steinhagen [22], the void fraction was estimated using Rouhani’s correlation [28]:

$$\alpha_n = \frac{x_n}{\rho_{g,n}} \left\{ [1 + 0.12(1 - x_n)](x_n/\rho_{g,n} + (1 - x_n)/\rho_{l,s}) + 1.18/(\dot{m}''_{total,n} \rho_{l,s}^{0.5}) [g\sigma(\rho_{l,s} - \rho_{g,n})]^{0.25} \right\}^{-1} \quad (25)$$

where the total mass flux and quality, respectively, are expressed as:

$$\dot{m}''_{total} = U_{l,s,n}[\rho_{l,s} + C_{in,n}(1 - \eta_n)] \quad (26)$$

$$x_n = (1 - \eta_n)(\rho_{l,s}/C_{in,n} + 1 - \eta_n)^{-1} \quad (27)$$

As was shown in part I, even with a crude estimate of the reaction rate, the forgoing equations could be applied using local values for η and ρ_g to obtain reasonable (for two-phase flow, at least) estimates of the total pressure drop.

The Nusselt number for two-phase flow, lacking any correlations specifically for heat transfer in air–water flow in chevron-PHEs, requires recourse to heat/momentum transfer analogies. In particular, Martin [19], Schlünder [29], and Abu-Khader [30] have found that a generalized form of the classical Lévêque solution could correlate heat transfer data obtained from chevron PHEs surprisingly well. Martin modified the original generalized Lévêque equation to fit experimental data for turbulent flow in industrial PHEs from several sources to obtain the following expression:

$$Nu_h = 0.122 Pr^{1/3} (\mu/\mu_w)^{1/6} [f Re^2 \sin(2\beta)]^{0.374} \quad (28)$$

Martin obtained the term $\sin(2\beta)$ by taking D_h/L to be the distance between two crossing corrugations. One may, plausibly, extend Martin’s adaptation of the generalized Lévêque solution to the case of two-phase flow by recognizing the agitation and mixing caused by the interaction between gas bubbles and a surrounding fluid is similar to that of turbulence [31]. The Lévêque solution is an asymptotic solution based on approximating the velocity profile in the vicinity of a solid wall as linear, a more involved discussion of which may be found in Ref. [32]. Since the only change here from Lévêque’s original analysis is the inclusion of the two-phase multiplier, one finds that $Nu_h = Nu_h(\Phi_{TP}^2 f Re_n^2)$. Without sufficient data to re-adjust the constants in Martin’s adaptation of the generalized Lévêque equation, we opted simply to insert the two-phase multiplier into the bracketed term in Eq. (28):

$$Nu_h = 0.122 Pr^{1/3} (\mu_{l,s}/\mu_{l,s,w})^{1/6} [f_{l,s} \Phi_{TP}^2 Re^2 \sin(2\beta)]^{0.374} \quad (29)$$

The exponent 0.374 and leading multiplier 0.122 are expected to require adjustment to better match multi-phase reacting flow in a chevron PHE. As long as the thermal boundary layer remains thin, as it would in turbulent flow or highly agitated two-phase flow, one can expect the Lévêque correlation to be an appropriate basis for two-phase flow correlations in chevron PHEs. Eq. (29) implies that the added presence of a gas phase, which will yield $\Phi_{TP}^2 > 1$, actually enhances heat transfer. Such enhancement was observed by Vlasogiannis et al. [27] in their study of heat transfer with air–water flow in a vertical chevron PHE. Based on their experiments, Vlasogiannis et al. reported enhancements in the values of heat transfer coefficient in all cases where air was injected with water at the inlet.

2.4. Numerical procedure

The transport equations were solved using the finite-volume method, with each channel being partitioned into equally sized cells. Eqs. (7) and (17)–(19) are integrated over each cell, where upon Gauss’ divergence theorem is used to change the volume integrals of the convective and diffusive terms into fluxes at the cell face. 1st order upwind differencing is used for the convective fluxes, and 2nd order central differencing is used for the diffusive fluxes. A grid resolution of 100 cells per channel was found to be sufficient to establish grid independence.

Addressing the nonlinear source terms in the species and energy equations require an iterative approach. The energy and species conservation equations are linearized about an initial guess, and decoupled to form two separate linear systems, which are subsequently solved using conventional sparse matrix techniques. The pressure field is updated at the end of each iteration. The solver code was written in Maple 13™, and the matrix inversion was performed using the built in *LinearSolve* function. For the simulations presented in this paper, convergence typically requires 50 iterations and 3 min of wall-clock time for execution.

3. Results and discussion

The numerical model described above was used to design and evaluate the performance of a “prototype” HEX reactor. The reactor consists of 7 channels, 3 of which carry the slurry, and 4 of which carry the thermal load. This layout is shown in Fig. 3. The geometric parameters, based off the Alfa Laval M3 PHE used in part I of this study, are shown in Table 1. The intent of this exercise is to first determine the dominant parameter (or parameters) governing reactor performance, and then to determine if the operating conditions required to achieve full conversion near atmospheric pressure conditions are indeed realistic.

Table 1
Geometric parameters for “prototype” PHE.

Parameter	Value
L	0.48 m
De	0.00468 m
W	0.10 m
Φ_{AE}	1.1
β	30°

The simulations that were performed in pursuit of these objectives assumed the slurry inlet temperature to be fixed at 335 K, such that the reaction will be initiated immediately. The mass loading of the AC was held at 8 kg/m^3 while systematically varying the slurry flow rate and inlet pressure. The slurry-side Reynolds number ranged from 5 to 16; Abu Kader [30] found the modified generalized L  v  que equation to be an appropriate Nusselt number correlation (in single-phase flow) at low Re for the chevron angle in Table 1, but no data exists to validate Eq. (29) for multi-phase flow under low Re conditions. The single-phase friction factor correlations in Eqs. (20)–(22) are also applicable to laminar flow, and are therefore appropriate for the flow conditions considered in the simulations. All thermophysical properties were assumed to remain constant, and were evaluated at the slurry inlet temperature. This particular AC mass loading was chosen based on a target endothermic heat rejection rate of 2 kW, assuming near total conversion. In the interest of obtaining conservative estimates for heat transfer, the viscosity correction term in Eq. (29) was neglected (i.e., the ratio was assumed to be unity). The load fluid temperature is held constant to better isolate the effects of slurry-side convection and reaction. The property values used for these simulations are shown in Table 2.

The volumetric reaction terms in Eqs. (17) and (19) require an estimation of the rate constant, κ , and the average particle size. As an approximate first estimate, the peak initial power data reported by Schmidt [7] was used, along with the assumption that the initial value of the average particle diameter was $\sim 1 \text{ mm}$. By performing the energy balance on a closed-system – representative of the reactor used by Schmidt – and using the reaction rate term from Eq. (15) in addition to assuming the slurry temperature is uniform, the instantaneous power rating is obtained from $\dot{w} = \Delta H A_{total} \kappa (P - P_{eq})^2$, where A_{total} is the total particle surface area in the reaction. P_{eq} is calculated at the fluid temperature using Eq. (15), and P is assumed to be the set point pressure. The value of \dot{w} was estimated from the peak power ratings reported by Schmidt at 60 °C with a set point of 400 torr and propylene glycol as the heat transfer fluid. The reasoning behind this assumption was that the 400 torr setpoint was reached quickly, offering a more accurate estimate of P ; and the maximum power occurs early in the experiment, meaning the AC is closest to the initial reactor temperature of 60 °C and thereby allowing more accurate estimation of P_{eq} . This calculation yields $\kappa = 2.4 \times 10^{-10} \text{ m}^{-2} \text{ kPa}^{-2}$, which was used in the simulations, discussed next.

Table 2
Thermophysical properties used in simulations.

Property	Value	Units	Source
k_{plate}	13.4	W/m K	[33]
k_{ls}	0.196	W/m K	[33]
$c_{p,ls}$	2700	J/kg K	[34]
μ_{ls}	8.4	mPa s	[35]
μ_g	0.012	mPa s	[33]
ρ_{ls}	1036	kg/m ³	[35]
ρ_p	780	kg/m ³	[6]
ΔH	2000	kJ/kg	[6]

3.1. Numerical predictions

One of the major concerns for open flow reactors is the low residence time in which the reaction must occur. This consideration places a limit on the amount of AC that can be fed into the reactor for a given set of operating conditions. The task, then, is to predict the maximum amount (or mass concentration) of AC that can potentially be reacted. There are three major competing factors that influence the tradeoff between conversion efficiency and overall power rating, which are: residence time/advection, channel-to-channel heat transfer, and reaction rate.

Fig. 5 displays conversion as a function of load side temperature for two different flow rates and different inlet pressures. Reducing the inlet pressure from 110 kPa to 102 kPa did not have a significant effect on the load temperature at which the AC was completely reacted, whereas increasing the slurry flow rate by threefold required the load temperature to be raised by $\sim 10 \text{ K}$ to achieve full conversion. The conversion efficiency becomes less sensitive to changes in the inlet pressure at higher flow rates. The shape of the conversion curves reveals two competing effects on the reaction rate; surface area, and equilibrium drop. The equilibrium drop, which is proportional to $(P_{eq} - P)^2$ increases with axial distance due to decrease in local pressure from hydrodynamic losses, and increase in equilibrium pressure as the slurry temperature rises. While these effects tend to accelerate the reaction, the decreasing particle surface area eventually begins to dominate the conversion behavior, causing the sensitivity to load temperature to severely diminish after $\sim 90\%$ conversion. In reality, such asymptotic behavior is unlikely to be observed since particle break up and changes in the surface morphology would have an increasingly prominent effect on the total solid surface area per unit volume of slurry.

As an additional figure of merit for assessing reactor performance, it is insightful to consider the fraction of the total heat rejected (Q_{load}) in the form of latent heat (Q_{latent}) as a supplement to the overall power rating. Ideally, the proportion of heat rejected to the thermo-chemical heat sink should be as high as possible. In Fig. 6, the ratio $\varepsilon = Q_{latent}/Q_{load}$ is plotted with respect to normalized load temperature, $T^* = (T_{ld} - 335 \text{ K}) / (T_{ld}^* - 335 \text{ K})$, where T_{ld}^* is the load temperature at which “full” conversion is attained (i.e., $1 - \eta \geq 0.95$). As with the conversion efficiency, the inlet pressure has little effect on ε as compared to the residence time. Increasing the flow rate tends to increase the total power rating, but at the expense of ε since higher load temperatures are required. Thus, the

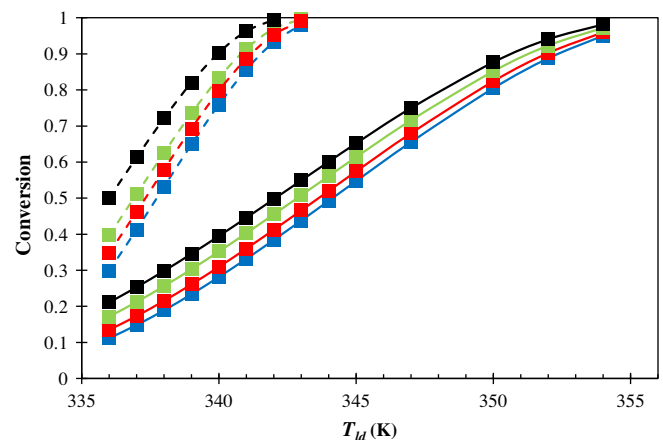


Fig. 5. Comparison of conversion efficiency (η) for slurry superficial velocities of 0.01 m/s (dashed line) and 0.03 m/s (solid line) as a function of load temperature for different inlet pressures: black – 102 kPa, green – 105 kPa, red – 108 kPa, and blue – 110 kPa. (For interpretation of the references to color in this figure legend, the reader is referred to the web version of this article.)

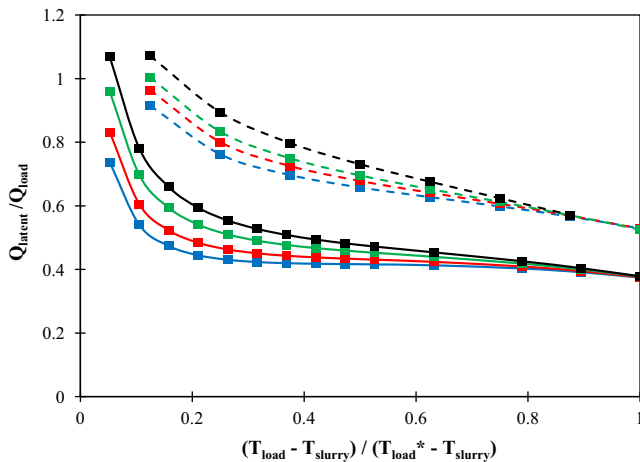


Fig. 6. Fraction of total heat rejected in the form of latent heat as a function of normalized load temperature for different inlet pressures: black – 102 kPa, green – 105 kPa, red – 108 kPa, and blue – 110 kPa. (For interpretation of the references to color in this figure legend, the reader is referred to the web version of this article.)

increase in Nu accompanying lower residence times is outweighed by the higher heat capacity rate.

For operating conditions close to atmospheric pressure conditions, the pressure losses are insufficient to supply the equilibrium pressure drop needed to bridge the gulf between the advection and reaction timescales, as evidenced by the greater load temperatures required at higher flow rates. It may be inferred from this fact that the global reaction rate is relatively insensitive to the axial variation of pressure (at least at the flow rates considered in this study), and is more sensitive to the axial variation in the slurry temperature.

From the standpoint of conversion efficiency and heat transfer, the residence time is the dominant parameter for operation close to atmospheric pressure conditions. Increasing the residence time permits a greater portion of the total heat load to be rejected to the AC, but the overall power rating is diminished. Additional plates may be added to the reactor to adjust the residence time to the appropriate level if one desires to react a greater quantity of AC by increasing the slurry flow rate. If the objective is to maximize the proportion of the thermal load rejected to the AC for a fixed PHE design, the residence times will need to be maximized to the greatest extent possible.

The instances where $\varepsilon > 1$ correspond to conditions when the reaction rate outpaces the rate of channel-to-channel heat transfer. Hence, the reaction consumes sensible heat from the slurry faster than it can be extracted from the load. Essentially, the AC is being wasted in this condition since it is primarily cooling the slurry rather than the hot stream fluid, as is evident in the axial temperature profiles in Figs. 7 and 8. On the vertical axes of Figs. 7 and 8, a new dimensionless temperature is defined as $\Theta = (T_s - 335 \text{ K}) / (T_{id} - 335 \text{ K})$, so that the effect of the endothermic reaction is readily apparent. The solid black curve, representing the case $T_{id} = 336 \text{ K}$, can be seen to increase before gradually decreasing when the inlet pressure is 110 kPa (Fig. 7). With the inlet pressure at 102 kPa (Fig. 8), the slurry temperature when $T_{id} = 336 \text{ K}$ actually falls below its inlet value, and stabilizes at approximately 334.8 K before slowly increasing again due to the increase in the heat transfer coefficient as the reaction progresses. It is desirable to have ε as close to unity as practically possible, since heat would be extracted from the load fluid at the same rate it is consumed by the endothermic reaction.

3.2. HEX reactor sizing calculations

As a benchmark for HEX reactor performance, the data obtained from the above simulations was used to estimate the size of a

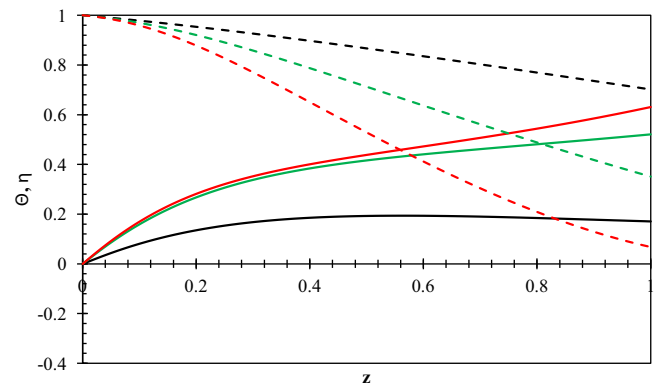


Fig. 7. Dimensionless axial temperature and concentration profiles for different load temperatures (black – 336 K, green – 339 K, red – 342 K) with $U_{ls} = 0.01 \text{ m/s}$, $C_{in} = 8 \text{ kg/m}^3$, and $P_{in} = 110 \text{ kPa}$. (For interpretation of the references to color in this figure legend, the reader is referred to the web version of this article.)

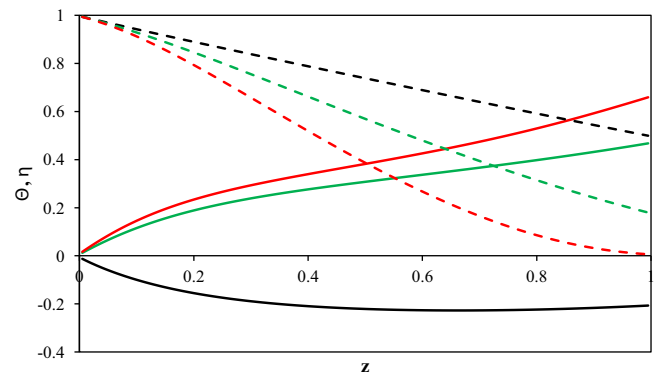


Fig. 8. Dimensionless axial temperature and concentration profiles for different load temperatures (black – 336 K, green – 339 K, red – 342 K) with $U_{ls} = 0.01 \text{ m/s}$, $C_{in} = 8 \text{ kg/m}^3$, and $P_{in} = 102 \text{ kPa}$. (For interpretation of the references to color in this figure legend, the reader is referred to the web version of this article.)

reactor and the required operating conditions to reject 2 kW of heat. Assuming that the heat rejection per channel is similar to that of a larger reactor (>20 plates), Table 3 shows the minimum reactor size for a 2 kW heat load based on operating conditions. The first four entries from the top are for the lowest residence time ($U_{ls} = 0.01 \text{ m/s}$), where over 50% of the total heat load is rejected to the AC; with 30–35 plates, the Alfa Laval M3 would occupy a volume of ~30 L with a footprint of 865 cm². The reactor would be roughly the same size as a typical desktop printer, and with an AC loading of 8 kg/m³, and consume about 0.7 g/s of solid AC. With the slurry temperature at 335 K, the required load temperature is, at most, 342 K, which is well below the industry standard safe limit for electronics cooling (358 K) [36]. The plate surface area is approximately 530 cm² (the actual area available for heat transfer may be lower since the corrugated section does not cover the entire plate), from which the heat load per plate q'' is derived.

Even with conservative estimates for thermal performance (neglecting viscosity correction and multiplier correction to Eq. (23)), the size and operating temperature requirements for a small-scale reactor are reasonable for operating conditions close to atmospheric. It is also clear that the tradeoff between residence time and total power rating means that increasing the specific heat duty of the reactor (heat load per unit system volume) causes depreciation in ε . In order to strike the appropriate balance between ε and the overall power rating will depend on the actual application and operating constraints.

Table 3Reactor size (minimum number of plates) required to reject 2 kW of waste heat; $\Delta T = T_{id} - 335$ K is the load–slurry temperature difference at the inlet.

Slurry flow rate (L/s)	Q_{latent} (W)	Q_{total} (W)	Q_{latent}/Q_{total}	ΔT (K)	P_{in} (kPa)	Min. plates	q'' (W/cm ²)
0.078	1114	2017	0.55	7.4	110	30	0.12
0.083	1185	2076	0.57	6.9	108	32	0.11
0.083	1185	2029	0.58	6.9	106	32	0.11
0.09	1293	2040	0.63	5.8	102	15	0.1
0.049	754	2015	0.37	19	110	6	0.58
0.056	862	2275	0.38	18.7	108	7	0.56
0.056	862	2228	0.39	18.1	105	7	0.55
0.056	862	2168	0.4	17.5	102	7	0.54

4. Conclusions

In order to provide a useful engineering analysis tool to predict HEX reactor performance, we have developed a reduced-order semi-empirical model since the analysis of multi-phase flows is still a heavily empirical practice [11]. The selection of empirical correlations for the void fraction and two-phase multiplier was guided by experimental data obtained in part I. As an initial feasibility study, a reduced-order reactor model was developed to ascertain the critical parameters governing the performance. The model was based on conventional correlations for plate heat exchangers. The numerical results show that the conversion efficiency and the proportion of the total heat transferred consumed by the chemical reaction are more strongly influenced by the residence time than the operating pressure. Furthermore, the designed reactor meets the constraints for size and operating temperatures while achieving the required thermal load. A thermal load of 2 kW is designed to be handled by a PHE with a footprint of only 30 L in volume with operating conditions close to atmospheric pressure.

Disclosure statement

To our knowledge, there are no conflicts of interest between the authors or their respective institutions with the International Journal of Heat and Mass Transfer.

References

- [1] E.C. Subbarao, R.A. Mashelkar, *Heat Transfer Equip. Des.* (1988) 227–254.
- [2] E. Santacesaria, M. Di Serio, R. Tesser, L. Casale, D. Verde, R. Turco, A. Bertola, Use of a corrugated plates heat exchanger reactor for obtaining biodiesel with very high productivity, *Energy Fuels* 23 (2009) 5206–5212.
- [3] A.M. Edge, I. Pearce, C.H. Phillips, Compact heat exchangers as chemical reactors for process intensification (PI), *Proc. Intens.* (1997) 175–189.
- [4] D. Johnson, S. Patnaik, J. Ervin, An integrated chemical reactor-heat exchanger based on ammonium carbamate, in: *Proceedings of the SAE 2012 Power Systems Conference*, SAE International, Phoenix, 2012.
- [5] J.R. García-Cascales, F. Vera-García, J. González-Maciá, J.M. Corberán-Salvado, M.W. Johnson, G.T. Kohler, Compact heat exchangers modeling: condensation, *Int. J. Refrig.* 33 (2010) 135–147.
- [6] H. Qiao, V. Aute, H. Lee, K. Saleh, R. Radermacher, A new model for plate heat exchangers with generalized flow configurations and phase change, *Int. J. Refrig.* 36 (2013) 622–632.
- [7] J.E. Schmidt, The use of ammonium carbamate as a high specific thermal energy density material for thermal management of low grade heat (MS thesis), University of Dayton, Dayton, OH, 2011.
- [8] J. Bellas, I. Chaer, S.A. Tassou, Heat transfer and pressure drop of ice slurries in plate heat exchangers, *Appl. Therm. Eng.* 22 (2002) 721–732.
- [9] Z.W. Ma, P. Zhang, Pressure drop and heat transfer characteristics of clathrate hydrate slurry in a plate heat exchanger, *Int. J. Refrig.* 34 (2011) 796–806.
- [10] M.C. Georgiadis, S. Macchietto, Dynamic modeling and simulation of plate heat exchangers under milk fouling, *Chem. Eng. Sci.* 55 (2000) 1605–1619.
- [11] V.P. Carey, *Liquid–Vapor Phase-Change Phenomena: An Introduction to the Thermophysics of Vaporization and Condensation Processes in Heat Transfer Equipment*, 1992, Taylor and Francis; Hebron.
- [12] N.P. Chermisinoff, R. Gupta, *Handbook of Fluids in Motion*, 1983, pp. 895–927, Ann Arbor Science Publishers; Ann Arbor.
- [13] B. Claudel, L. Boulamri, A new model of gas–solid kinetics: the case of ammonium carbamate formation and decomposition, *Thermochim. Acta* 126 (1988) 129–148.
- [14] A.A. Koutinas, P. Yianoulis, A. Lycourghiotis, Industrial scale modelling of the thermochemical energy storage system based on CO_2 2NH_3 $\text{NH}_2\text{COONH}_4$ equilibrium, *Energy Convers. Manage.* 23 (1983) 55–63.
- [15] R.N. Bennet, P.D. Ritchie, D. Roxburgh, J. Thomson, The system ammonia carbon dioxide ammonium carbamate. Part I. – the equilibrium of thermal dissociation of ammonium carbamate, *Trans. Faraday Soc.* 49 (1953) 925–929.
- [16] E.P.J. Egan, J.E.J. Potts, G.D. Potts, Dissociation pressure of ammonium carbamate, *Ind. Eng. Chem.* 38 (1946) 454–456.
- [17] T.R. Briggs, V. Migrdichian, The ammonium carbamate equilibrium, *J. Phys. Chem.* 28 (1924) 1121–1135.
- [18] H. Lu, N. Mazet, B. Spinner, Modeling of gas–solid reaction – coupling of heat and mass transfer with chemical reaction, *Chem. Eng. Sci.* 51 (1996) 3829–3845.
- [19] H. Martin, A theoretical approach to predict the performance of chevron-type plate heat exchangers, *Chem. Eng. Process. Process Intensif.* 35 (1996) 301–310.
- [20] W.W. Focke, J. Zachariades, The effect of the corrugation inclination angle on the thermohydraulic performance of plate heat exchangers, *Int. J. Heat Mass Transfer* 28 (1985) 1469–1479.
- [21] W.W. Focke, P.G. Knibbe, Flow visualization in parallel-plate ducts with corrugated walls, *J. Fluid Mech.* 165 (1986) 73–77.
- [22] G. Kreissig, H.M. Müller-Steinhagen, Frictional pressure drop for gas/liquid two-phase flow in plate heat exchangers, *Heat Transfer Eng.* 13 (1992) 42–52.
- [23] C. Tribbe, H.M. Müller-Steinhagen, Gas/liquid flow in plate-and-frame heat exchangers – part I: pressure drop measurements, *Heat Transfer Eng.* 22 (2001) 5–11.
- [24] C. Tribbe, H.M. Müller-Steinhagen, Gas/liquid flow in plate-and-frame heat exchangers – part II: two-phase multiplier and flow pattern analysis, *Heat Transfer Eng.* 22 (2001) 12–21.
- [25] Y. Shiomi, S. Nakanishi, T. Uehara, Characteristics of two-phase flow in a channel formed by chevron type plates, *Exp. Therm. Fluid Sci.* 28 (2004) 231–235.
- [26] K. Nilpueng, S. Wongwises, Two-phase gas–liquid flow characteristics inside a plate heat exchanger, *Exp. Therm. Fluid Sci.* 34 (2010) 1217–1229.
- [27] P. Vlasogiannis, G. Karagiannis, P. Argyropoulos, V. Bontozoglou, Air–water two-phase flow and heat transfer in a plate heat exchanger, *Int. J. Multiphase Flow* 28 (2002) 757–772.
- [28] S.Z. Rouhani, E. Axelsson, Calculation of void volume fraction in the subcooled and quality boiling regions, *Int. J. Heat Mass Transfer* 13 (1970) 383–393.
- [29] E.-U. Schlünder, Analogy between heat and momentum transfer, *Chem. Eng. Process. Process Intensif.* 37 (1998) 103–107.
- [30] M. Abu-Khader, Better thermal calculations using modified generalized Leveque equations for chevron plate heat exchangers, *Int. J. Green Energy* 4 (2007) 351–366.
- [31] Y. Sato, K. Sekoguchi, Liquid velocity distribution in two-phase bubble flow, *Int. J. Multiphase Flow* 2 (1975) 79–95.
- [32] A.S. Jones, Heat transfer in the thermal entrance region of a flat duct, *J. Aust. Math. Soc. Ser. A Pure Math. Stat.* 19 (1975) 146–160.
- [33] F.P. Incropera, D.P. Dewitt, T.L. Bergman, A.S. Lavine, *Fundamentals of Heat and Mass Transfer*, sixth ed., John Wiley and Sons, New Jersey, 2007.
- [34] P.L. Geiringer, *Handbook of Heat Transfer Media*, Reinhold Publishing Corp, New York, 1962.
- [35] T. Sun, A.S. Teja, Density, viscosity, and thermal conductivity of aqueous solutions of propylene glycol, dipropylene glycol, and tripropylene glycol between 290 K and 460 K, *J. Chem. Eng. Data* 49 (2004) 1311–1317.
- [36] I. Mudawar, Assessment of high-heat-flux thermal management schemes, *IEEE Trans. Compon. Packag. Technol.* 24 (2001) 122–141.